

## Research Article

# In Silico, SwissADME, and DFT Studies of Newly Synthesized Oxindole Derivatives Followed by Antioxidant Studies

Abdur Rauf <sup>1</sup>, Haroon Khan <sup>1</sup>, Momin Khan <sup>2</sup>, Ali Abusharha <sup>3</sup>,  
Goncagül Serdaroglu <sup>4</sup> and Maria Daglia <sup>5,6</sup>

<sup>1</sup>Department of Pharmacy, Abdul Wali Khan University Mardan, Mardan 23200, Pakistan

<sup>2</sup>Department of Chemistry, Abdul Wali Khan University Mardan, Mardan 23200, Pakistan

<sup>3</sup>Optometry Department, Applied Medical Sciences College, King Saud University, P. O. Box 145111, Riyadh, Saudi Arabia

<sup>4</sup>Sivas Cumhuriyet University, Mathematics and Science Education, Sivas 58140, Türkiye

<sup>5</sup>Department of Pharmacy, University of Naples Federico II, Naples, Italy

<sup>6</sup>International Research Centre for Food Nutrition and Safety, Jiangsu University, Zhenjiang 212013, China

Correspondence should be addressed to Haroon Khan; haroonkhan@awkum.edu.pk

Received 27 July 2023; Revised 17 November 2023; Accepted 25 November 2023; Published 12 December 2023

Academic Editor: Mahmood Ahmed

Copyright © 2023 Abdur Rauf et al. This is an open access article distributed under the Creative Commons Attribution License, which permits unrestricted use, distribution, and reproduction in any medium, provided the original work is properly cited.

The compounds were synthesized by refluxing 6-chlorooxindole with 2,3-dichlorobenzaldehyde and 2,6-dichlorobenzaldehyde in the presence of piperidine as a catalyst and characterized by spectroscopic analysis using <sup>1</sup>H NMR, <sup>13</sup>C NMR, and mass spectrometry as (E)-3-(2,3-dichlorobenzylidene)-6-chloroindolin-2-one (C-1) and (E)-3-(2,6-dichlorobenzylidene)-6-chloroindolin-2-one (C-2). Additionally, in silico ADME studies indicated that C-1 and C-2 with 1,1 rotatable bonds could have moderate water solubility and therefore could have the potential ability to cross the blood-brain barrier. Both showed high GI absorption, indicating that they are suitable for intestinal absorption while the compounds showed CYP1A2, CYP2C19, and CYP2C9 inhibition. The five drug-likeness criteria, which were Lipinski, Muegge, Ghose, Veber, and Egan, and the principles of drug-likeness are not violated by compounds C-1 and C-2. Also, the DFT computations were performed at the B3LYP level and at 6-311++G\*\* basis set to evaluate and support the obtained results from the experiment. The FMO results revealed that C-1 could likely prefer the intramolecular interactions rather than the intermolecular interactions, and vice versa for C-2. In addition, the NBO results indicated that the resonance interaction, especially the shift of electron to empty orbitals from lone pair electrons of nitrogen, would contribute to the stabilization of both compounds greatly. In DPPH assay, the compounds showed IC<sub>50</sub> values of 37.390 and 34.676 μM, respectively. Similarly, in ABTS assay, the calculated IC<sub>50</sub> values for the compounds were 25.381 and 33.706 μM, respectively. In short, these results provided a solid ground for further preclinical studies in quest of new effective therapeutic agents.

## 1. Introduction

Oxindoles are endogenous aromatic organic compounds that are present in some plant natural products as well as in the tissues and bodily fluids of mammals. They have a bicyclic structure and are aromatic heterocyclic organic compounds. The unsubstituted oxindole nucleus is characterized as an off-white crystalline powder with a defined melting point range of 124–126°C [1, 2]. The fusion of a nitrogen-containing five-membered ring with a six-membered benzene ring results in

the formation of an oxindole molecule. The structure of an oxindole is similar to that of an indoline, with the exception that one of the five members' 2-positions is occupied by a carbonyl [3]. According to the literature, oxindole has been used to treat inflammation, cancer, gastric ulcers, infections, and other medical conditions [4]. The diverse pharmacological profile of oxindole has inspired both industry and academia to create novel synthetic derivatives with a wide range of biological activities. The development of synthetic oxindole derivatives has played a crucial role in the creation of sunitinib,

a commercialized anticancer drug used to treat metastatic renal cell cancer and gastrointestinal stromal tumors [5]. Alkaloids in the form of the first known oxindole derivative have been naturally extracted from the bark of the tropical climber plant cat's claw (*Uncaria tomentosa*).

The compound "oxindole" and its derivatives, in both keto-enol tautomeric forms, are referred to as "1,3-dihydro-2H-indole-2-one(s)" by the IUPAC (International Union of Pure and Applied Chemistry) due to their structural composition, which is composed of a fused six-membered benzene ring and a five-membered pyrrole ring, along with a carbonyl group located at the C-2 position. In this context, lactam-lactim interconversion used as a tool for the synthesis of complex molecules in organic chemistry is an important kind of tautomerism that denotes the shifting of hydrogen between the nitrogen atom and the oxygen atom in such heterocyclic bicyclic rings. Thus, the nomenclature of oxindole is considered as 2-indolinone being one of the indole derivatives [6], and the characteristic peak of oxindole in the mass spectrum has appeared at  $m/z$  133 (100%). The tautomeric form of oxindole is typically represented as the lactam (I') of o-aminophenyl acetic acid. The other forms are enol form (I'''), which has H of CH<sub>2</sub> group tautomerase, and lactim form (I''), which has H of N tautomerism [1].

As known well, "reactive oxygen species" (ROS) and "reactive nitrogen species" (RNS) are the two main types of free radicals that can be produced via internal (mitochondria, the endoplasmic reticulum, phagocytic cells, etc.) and external sources (pollution, smoke, alcohol, etc.). Both ROS and RNS, when levels of ROS and RNS are kept in balance in the body, can play important roles in normal cellular signaling and immune system function, but they can also cause damage to cells and tissues by reacting with and damaging cellular components such as lipids, proteins, and DNA.

However, if there occurs imbalance in the level of both ROS and RNS, they can cause the development of diseases such as cancer, cardiovascular disease, and neurodegenerative diseases [6].

The oxindole molecule inhibited oxidative stress-related cell death, especially ferroptosis and oxytosis caused by glutamate and erastin, respectively [7]. For the discovery of a new therapeutic class, the oxindole derivatives may be evaluated as viable candidates [8]. Until now, computational methods and applications were implemented very satisfactorily in molecular systems from organic [9] to complex molecules [10] to explore the intrinsic feature of the systems underlying the key reactivity trend.

In this connection, the current article deals with the synthesis of a couple of oxindoles derivatives, which were characterized using various spectroscopic techniques as compounds C-1 and C-2. The synthesized compounds were evaluated for the physicochemical properties, and pharmacokinetic profile through SwissADME. Similarly, the computations of this study has been employed by the B3LYP/6-311++G\*\* level for the elucidation of the possible reactivity attitude and sites of the synthesized compounds. Moreover, the compounds were also subjected to various in vitro free radical scavenging tests.

## 2. Materials and Methods

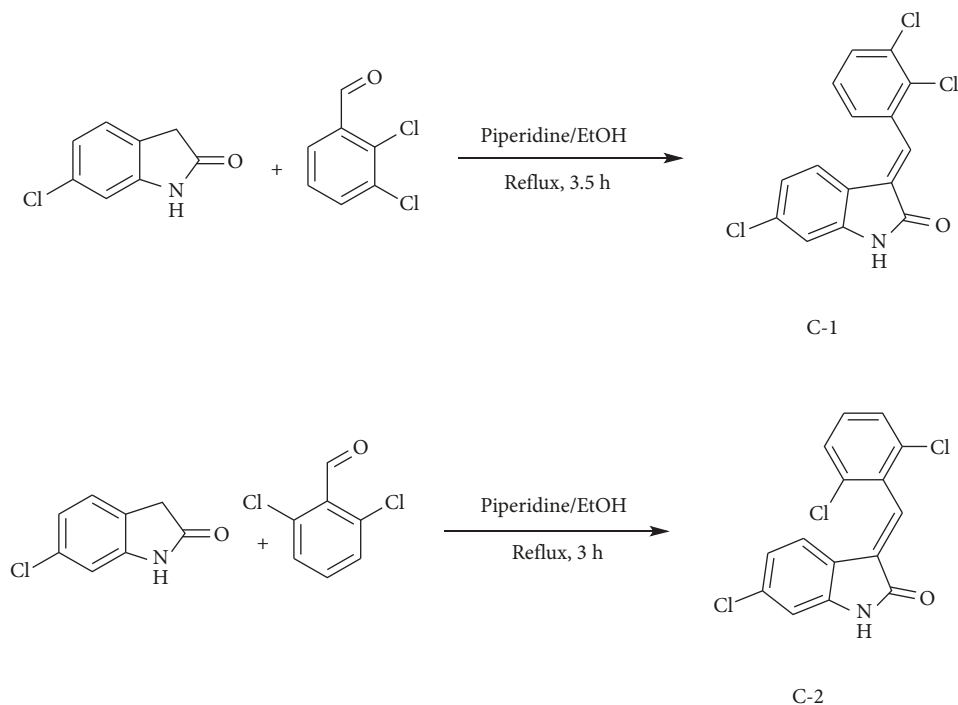
**2.1. Synthesis of Compounds.** Synthesis of the selected compounds was carried out via refluxing 6-chlorooxindole with 2,3-dichlorobenzaldehydes and 2,6-dichlorobenzaldehydes in ethanol and piperidine as a catalyst quantity, respectively (Scheme 1). The reaction mixture was refluxed for 3.5 and 3 hours. After the completion of reactions as determined by TLC analysis, the materials were cooled and concentrated at reduced pressure that led to solid 3-oxindole derivatives C-1 and C-2. The products were washed with equal volumes of a mixture of hexane-ethyl acetate (25 mL) and dried to afford desired compounds [11]. <sup>1</sup>H NMR, <sup>13</sup>C NMR, and HR ESI mass spectroscopy were used for the determination of their structures. Rf values, isolated yields of the pure-produced compounds, and the compounds' physical characteristics were all documented individually.

**2.2. Characterization.** Rf values, isolated yields of the pure-produced compounds, and the compounds' physical characteristics were all documented individually. Mass spectroscopy and nuclear magnetic resonance (<sup>1</sup>H and <sup>13</sup>C NMR) were utilized to determine the structures of the produced compounds.

**2.2.1. (E)-3-(2,3-Dichlorobenzylidene)-6-chloroindolin-2-one (C-1).** Yield: (89%); <sup>1</sup>H NMR (600 MHz, DMSO-*d*<sub>6</sub>): δ 10.33 (s, 1H, NH), 7.57 (s, 1H, =CH), 7.35 (m, 2H, H-4'/4), 7.29 (t, 1H, *J*<sub>5'(4',6')</sub> = 7.8 Hz, H-5'), 7.30 (d, 1H, *J*<sub>5,4</sub> = 8.0 Hz, H-5), 6.99 (d, 1H, *J*<sub>6',5'</sub> = 8.5 Hz, H-6'), 7.03 (d, 1H, *J*<sub>7,5</sub> = 8.0 Hz, H-7); <sup>13</sup>C NMR (150 MHz, DMSO-*d*<sub>6</sub>): δ 175.4, 145.0, 142.5, 132.2, 131.0, 129.0, 128.4, 128.2, 127.3, 125.2, 120.8, 124.1, 121.3, 120.8, and 119.2; HRESI-MS [M+H]<sup>+</sup> calcd for 323.970, found 323.976. Specific spectroscopic details can be found in the supplementary materials (Figures S1 and S2).

**2.2.2. (E)-3-(2,6-Dichlorobenzylidene)-6-chloroindolin-2-one (C-2).** Yield: (90%); <sup>1</sup>H NMR (600 MHz, DMSO-*d*<sub>6</sub>): δ 10.88 (s, 1H, NH), 7.62 (s, 1H, =CH), 7.60 (d, 1H, H-7), 7.51-7.44 (m, 2H, Hz, H-4'/5'), 6.87-6.83 (m, 3H, H-3'/4/5); <sup>13</sup>C-NMR (150 MHz, DMSO-*d*<sub>6</sub>): δ 167.4, 144.3, 135.1, 133.2, 132.1, 131.4, 130.8, 129.0, 128.7, 124.1, 121.5, 119.6, and 110.3; [M+H]<sup>+</sup> calcd for 323.970, found 323.978. Specific details can be found in the supplementary materials (FS-24 and FS-24 mass spectra).

**2.2.3. Studies on Pharmacokinetics.** The idea of drug-like chemical species is widely utilized in drug discovery and candidate selection. Compounds that possess pharmacokinetic properties suitable for persisting throughout human-phase clinical trials are considered to belong to drug-like chemical species [12]. The SwissADME database [13, 14] was employed to evaluate the physicochemical properties, pharmacokinetic profile, drug similarity, and medicinal chemistry of the compounds, including their lipophilicity and water solubility [15]. The 2D structures from the



SCHEME 1: Synthesis of oxindole derivatives C-1 and C-2.

database were converted into a string-based search format, allowing for efficient screening and analysis of potential drug candidates (Table 1).

**2.3. DFT Computational Study.** The G09W [12] and GaussView 6.0.16 [13, 15] packages were used for all computations and visualizations of the optimized molecule geometries and FMO graphs, respectively. All computational efforts of the compounds were made at the B3LYP [14]/6-311++G\*\* level [16]. The second-order perturbative energy analysis [17] was conducted by the NBO code [18] implemented in the G09W package. The energy lowering for a specific interaction depending on the  $q_i \rightarrow$  “bonding orbital occupancy,”  $\epsilon_i$  and  $\epsilon_j \rightarrow$  “bonding and antibonding orbital energies” (diagonal elements), and  $F_{ij} \rightarrow$  the off-diagonal NBO Fock matrix element is defined as follows:

$$E^{(2)} = \Delta E_{ij} = q_i \frac{(F_{ij})^2}{(\epsilon_j - \epsilon_i)}. \quad (1)$$

The  $I$  ionization energy” and  $A$  “electron affinity” are approximated [19] via the HOMO and LUMO energies.

$$\begin{aligned} I &= -E_{\text{HOMO}}, \\ A &= -E_{\text{LUMO}}. \end{aligned} \quad (2)$$

Then, “ $I$ ” and “ $A$ ” values are used to get the reactivity tensors [20, 21] by the following formulae equations:

$$\begin{aligned} \chi &= \frac{I + A}{2}, \\ \eta &= \frac{I - A}{2}, \\ \omega &= \frac{\mu^2}{2\eta}, \end{aligned} \quad (3)$$

$$\Delta N_{\text{max}} = \frac{I + A}{2(I - A)}.$$

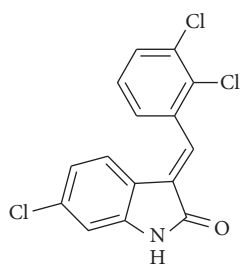
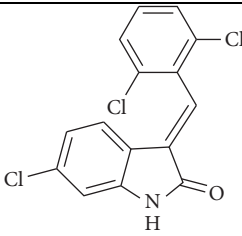
The terms are stated as  $\chi \rightarrow$  “electronic chemical potential,”  $\eta \rightarrow$  “global hardness,”  $\omega \rightarrow$  “electrophilicity,” and  $\Delta N_{\text{max}} \rightarrow$  “maximum charge transfer capability.”

Last, the  $\omega^-$  “the electron donating power” and  $\omega^+$  “the electroaccepting power” [22], and  $\Delta E_{\text{back-donat}}$  “back-donation energy” [23] values are also computed approximately by using the “ $I$ ” and “ $A$ ” values.

$$\begin{aligned} \omega^+ &\approx \frac{(I+3A)^2}{(16(I-A))}, \\ \omega^- &\approx \frac{(3I+A)^2}{(16(I-A))}, \end{aligned} \quad (4)$$

$$\Delta \epsilon_{\text{back-donation}} = -\frac{\eta}{4}.$$

TABLE 1: IUPAC name and chemical structures of the studied oxindoles (C-1 and C-2).

Ligand	IUPAC name	Structure
C-1	(E)-3-(2,3-Dichlorobenzylidene)-6-chloroindolin-2-one	
C-2	(E)-3-(2,6-Dichlorobenzylidene)-6-chloroindolin-2-one	

The electron and hole density distributions (EDD and HDD) are estimated by using the molecular orbital (MO) wave function ( $\Phi$ ) and the configuration coefficient ( $w$ ), which represent the transition of an electron from an occupied MO ( $i$ ) to a virtual MO ( $j$ ), as shown in the following equations:

$$\begin{aligned} \rho_{ele}(r) &= \sum iw_i \Phi_i(r)^2 \Phi_j(r)^2, \\ \rho_{hole}(r) &= \sum iw_i \Phi_i(r). \end{aligned} \quad (5)$$

Total electron density is quantified by the following equation:

$$\frac{1}{4} \nabla^2 p(r) = G(r) + \gamma \{r\}, \quad (6)$$

where  $G(r)$  and  $V(r)$  are Lagrangian kinetic energy and potential energy densities at critical points, respectively.

#### 2.4. Antioxidant Studies

**2.4.1. DPPH Scavenging Assay.** The potential of test compounds to neutralize free radicals was scrutinize using 1,1-diphenyl-2-picrylhydrazyl (DPPH) radicals [24]. Briefly, five dilutions of each synthesized compound including 62.5, 125, 250, 500, and 1000  $\mu$ l were prepared. It was followed by the addition of 0.1 ml of each dilution to methanol diluted  $4 \times 10^{-3}$ % solution of DPPH [2]. The positive control was ascorbic acid. Calculating scavenging activity as a percentage, the following equation is derived:

$$\% \text{ Scavenging effect} = \frac{[A_0 - A_1]}{A_0} \times 100, \quad (7)$$

where  $A_0$  is the absorbance of the control and  $A_1$  is the absorbance of the compound sample. Every experiment was run in triplicate, and median inhibitory doses ( $IC_{50}$ ) values were calculated by using SPSS.

**2.4.2. ABTS Scavenging Assay.** The antioxidant activity of the test compounds was also assayed using ABTS (2,2-azino-bis [3-ethylbenzthiazoline]-6-sulfonic acid) free radicals. Here, the antioxidant activity is represented by the scavenge potential on  $ABTS^+$  radical cation, causing down shift in absorbance at 734 nm, provides the basis for the action. The radical solutions (7 mM) and  $K_2S_2O_8$  (2.45 mM) were made and added. At room temperature, the resulting mixture was kept in the dark (12–16 h), formed a dark-colored solution carrying  $ABTS^+$ . The phosphate buffer (0.01 M, pH 7.4) was used to dilute the  $ABTS^+$  radical cation solution in order to achieve an absorbance value of 0.70 at 734 nm at the time of activity. The compounds' ability to scavenge radicals was tested by mixing 3.0 mL of the ABTS solution with 3  $\mu$ L of each sample dilution (62.5, 125, 250, 500, and 1000  $\mu$ L) of the compounds. Following the one-minute mixing of the solutions, the decrease in absorbance was recorded for six minutes using spectrophotometry. The positive control was ascorbic acid. The assay was carried thrice, and a formula was used to compute the % inhibition:

$$\% \text{ scavenging effect} = \frac{[\text{control absorbance} - \text{sample absorbance}]}{\text{control absorbance}} \times 100. \quad (8)$$

The percent inhibition and  $IC_{50}$  values were determined to present the effects [24].  $IC_{50}$  was calculated using SPSS, and results were interpreted.

**2.5. Statistical Analysis.** Statistical analysis was performed by using SPSS. Every experiment was run in triplicate, and median inhibitory doses ( $IC_{50}$ ) values were calculated using SPSS.  $P < 0.05$  was considered as the level of significance.

### 3. Results

**3.1. Evaluation of Physicochemical Characteristics.** Both the compounds C-1 and C-2 (Figure 1), comply with Lipinski's rule. This suggests that their molecular makeup is similar to that of oral medicines (Table 2). All oxindole derivatives are within the established ranges of  $\leq 500$ ,  $\leq 5$ ,  $\leq 140 \text{ \AA}^2$ , and  $\leq 10$ , respectively, for molecular weight (MW), the number of hydrogen bond donors (nHBD), topological polar surface area (TPSA), logP, and the number of hydrogen bond acceptors (nHBAs). For the oxindole derivatives C-1 and C-2, the F. Csp3 values are the same as 0.00 s (Table 2). Both oxindole derivatives feature 1,1 rotatable bond, which is similar. The molar refractivity was discovered to be the same as 87.17.

**3.2. Lipophilicity and Water Solubility.** The partition of the oxindole derivatives C-1 and C-2 preferred into the water compartment, is shown by their log Po/w values, which ranged from 4.33 to 4.34. Both the compounds C-1 and C-2 are predicted as moderately soluble. For the C-1 and C-2 compounds, Log S is aqueous solubility and has the same value of  $-5.12$ , which is less than the specified range of  $-4$  to  $0.5 \text{ log mol/L}$ , as indicated (Table 3).

**3.3. Characteristics of Pharmacokinetics.** Pharmacokinetics is crucial to obtain the intended pharmacological outcome of a drug. This suggests that every compound's pharmacokinetic characteristic has the potential to impact a drug's pharmacological profile. High GI absorption was found for both substances C-1 and C-2 derivatives according to the SwissADME database. Figures 2 and 3 indicate the boiled-egg graphs for C-1 and C-2, respectively. Both the oxindole derivatives C-1 and C-2 demonstrated strong GI absorption, indicating that they are suitable for intestinal absorption. Both the C-1 and C-2 derivatives of oxindole can pass the blood-brain barrier. Compounds C-1 and C-2 are not substrates for P-glycoprotein (Table 4).

In the case of drug metabolism, C-1 and C-2 were discovered to be CYP1A2, CYP2C19, and CYP2C9 inhibitors. CYP2D6 and CYP3A4 are unaffected by compounds C-1 and C-2. The bioavailability score for C-1 and C-2 oxindole derivatives is 0.55, which is similar.

**3.4. Drug-Likeness.** According to Table 5, the five drug-likeness approaches (Lipinski, Muegge, Ghose, Veber, and Egan) are not violated by the compounds C-1 and C-2.

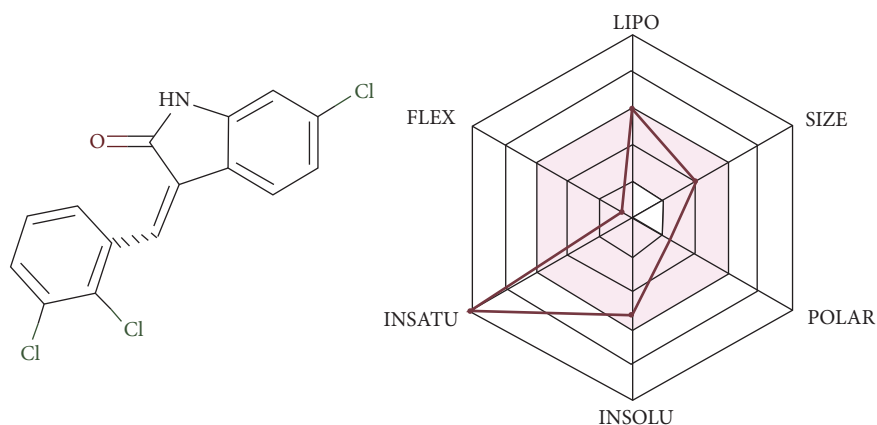
**3.5. Medicinal Chemistry.** The oxindole derivatives (C-1 and C-2) have no PAINS alert, without  $\alpha$ -screen artifacts and frequent hitters, and with reasonable reactivity. Brenk-structural-alert indicated a couple of reactive groups in these selected oxindole derivatives with Michael acceptor and stilbene. Compounds C-1 and C-2 have  $MW < 350$ , so they have lead likeness capability. Oxindole derivatives had scores of 2.52 and 2.55 in the SwissADME database, which are indicative of simple step reactions in synthesis.

**3.6. DFT Computations.** The optimized geometries and FMOs amplitudes of compounds C-1 and C-2 are presented in Figure 4. Table 6 presents the computed thermochemical quantities and reactivity parameters of the compounds.

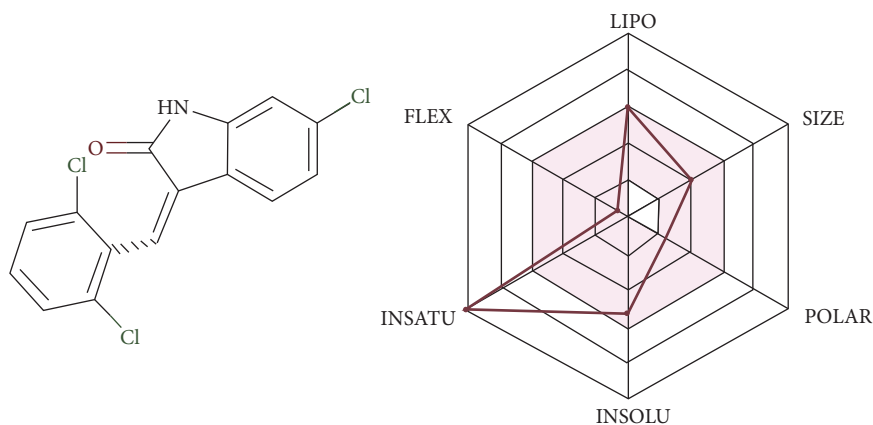
In terms of the stability of the molecules, it could be seen from Table 6 that the position of the second chlorine atom substituted on the benzene ring affected the molecular stability. Namely, the chlorine substitution on the 3-position of benzene made the compound C-1 more stable than the C-2 with chlorine substitution on the 6-position of the benzene ring. The  $\Delta E$ ,  $\Delta H$ , and  $\Delta G$  quantities (in au) of C-1 were calculated as  $-2087.061203$ ,  $-2087.043669$ , and  $-2087.108101$ , respectively, while these quantities of C-2 were found to be  $-2087.060467$ ,  $-2087.042719$ , and  $-2087.107219$ . Also, the position of the second chlorine on the structure affected the thermal energies; the  $\Delta E_{\text{thermal}}$  (kcal/mol) order of the compounds was determined as C-1 (130.145) > C-2 (129.694). The entropy of the compounds was predicted as C-1 (135.608) < C-2 (135.751), which implied that the C-2 molecule would be slightly more disordered than the C-1 molecule. Also, the DM and  $\alpha$  values of C-1 were calculated, at 1.099939 D and 261.327036, as greater than those of the C-2.

Also, the HOMO (eV) of C-2 was lower than that of C-1, of which order was as C-1 ( $-6.320$ ) < C-2 ( $-6.385$ ), while the LUMO (eV) of C-1 was lower than that of C-2 and calculated as C-1 ( $-2.988$ ) < C-2 ( $-2.563$ ).  $\Delta E$  (L-H) values indicated that C-1 could likely prefer the intramolecular interactions rather than the intermolecular interactions, and vice versa for C-2. Namely,  $\Delta E$  (eV) order of the compounds was calculated as C-1 (3.332) < C-2 (3.822). In terms of the electronic chemical potential and hardness of the compounds,  $\mu$  and  $\eta$  (eV) descriptors were found to be C-1 ( $-4.654$ ) > C-2 ( $-4.474$ ) and C-2 (1.666) > C-1 (1.911), respectively. From Table 6, the electrophilic character of C-1 was greater than C-2, and  $\omega$  (eV) order was determined as C-2 (0.239) > C-1 (0.192). Furthermore, the orders of  $\omega^+$  (au) and  $\omega^-$  (au) values of the compounds were determined as C-1 (0.161) > C-2 (0.119) and C-1 (0.332) > C-2 (0.283). Accordingly, the electrodonating and electroaccepting capabilities of C-1 are higher than those of C-2.  $\Delta \epsilon_{\text{back-donat}}$  (eV) values indicated that C-2 ( $-0.478$ ) would have gained stability more than C-1 ( $-0.417$ ) via back donation.

From Figure 4, the presence of chlorine at the 6-position for C-2 shifted the HOMO electron density towards the indoline ring, while HOMO for C-1 was expanded over almost the entire benzene surface. On the other hand,



SMILES Clc1ccc2c(c1)NC(=O)/C(=C/c1ccc(c1Cl)Cl



SMILES Clc1ccc2c(c1)NC(=O)/C(=C/c1c(Cl)cccc1Cl

FIGURE 1: The radar charts of compounds C-1 and C-2 depending on the physicochemical properties.

TABLE 2: The physicochemical property of oxindole (C-1 and C-2) derivatives calculated with the SwissADME database.

Ligands	Molecular formula	MW (g/mol)	nHA	nAHA	F.Csp <sup>3</sup>	nRB	nHBA	nHBD	MR	TPSA (Å <sup>2</sup> )
C-1	C <sub>15</sub> H <sub>8</sub> Cl <sub>3</sub> NO	324.59	20	12	0.00	1	1	1	87.17	29.10
C-2	C <sub>15</sub> H <sub>8</sub> Cl <sub>3</sub> NO	324.59	20	12	0.00	1	1	1	87.17	29.10

MW: molecular weight; nHA: no. of heavy atom; nAHA: no. of arom. heavy atom; F.Csp<sup>3</sup>: no. of sp<sup>3</sup> hybridized carbon out of total carbon count; nRB: no. of rotatable bonds; nHBA: no. of H-bond acceptors; nHBD: no. of H-bond donors, MR: molar refractivity; TPSA: topological polar surface area.

TABLE 3: The characteristics of lipophilicity and water solubility of oxindoles (C-1 and C-2).

Ligands	Lipophilicity			Water solubility			
	Consensus Log P <sub>o/w</sub>	Log S (ESOL)	Solubility class	Log S (Ali)	Solubility class	Log S (SILICOS-IT)	Solubility class
C-1	4.33	-5.24	Moderately soluble	-5.12	Moderately soluble	-7.26	Poorly soluble
C-2	4.34	-5.24	Moderately soluble	-5.12	Moderately soluble	-7.26	Poorly soluble

LUMO for C-1 was located on both chlorines positioned at 2- and 3-, while for C-2, it was not expanded on the 6-positioned chlorine. For both compounds, the surround of the oxygen atom was pointed out to the electron-rich region that was signed by red color ( $V < 0$ ). As expected, the

secondary amine hydrogen belonging to the indoline part of the compound was overlaid by blue ( $V > 0$ ), which represented the electron-poor region. The chlorine of both compounds was covered by a very light blue close to green which indicated they could have presented a neutral attitude.

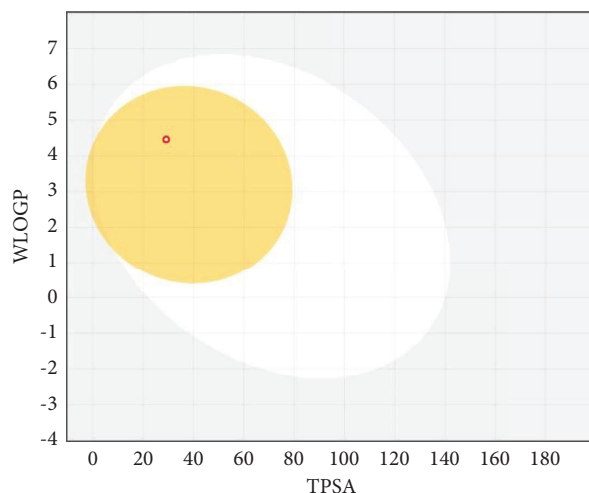


FIGURE 2: Boiled-egg representation of C-1.

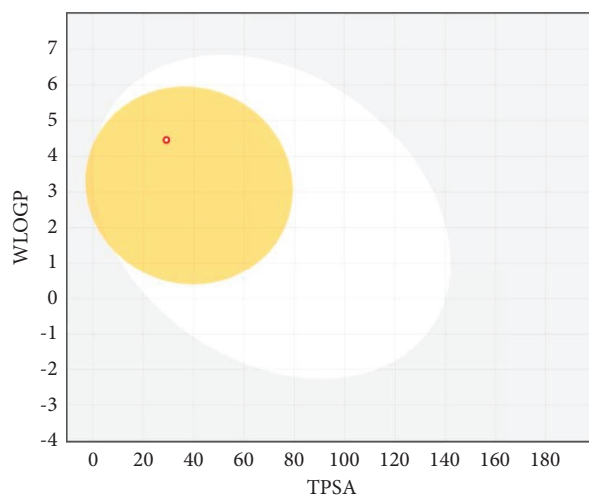


FIGURE 3: Boiled-egg representation of C-2.

TABLE 4: The bioavailability scores and pharmacokinetics of oxindole (C1 and C2) derivatives calculated with SwissADME database.

Ligands	GI abs	Bioavail. Score	BBB per	P-gp substrate	CYP1A2 inh	CYP2C 19 inh	CYP2C9 inh	CYP2D6 inh	CYP3A4 inh
C-1	High	0.55	Yes	No	Yes	Yes	Yes	No	No
C-2	High	0.55	Yes	No	Yes	Yes	Yes	No	No

But they would have been able to change the charge density on the oxygen and benzene ring via inductive effect.

**3.7. Natural Bond Orbital Study.** The results of the NBO analysis have been very informative to enlighten the possible electronic movements in the molecular systems from the organic-based to complex systems [25, 26] and thus consideration of the intrinsic reason underlying the possible reactivity potency of the systems. In this context, the possible electronic interactions taking place in the compounds were determined and summarized in Table 7.

The  $n-\pi^*$  interactions, especially the electron movement to unfilled orbitals from lone pair electrons of nitrogen, would contribute to the stabilization of both compounds,

greatly. The energies of the resonances LP (1) N3  $\rightarrow$   $\pi^*$  O2-C7 ( $ED_j=0.30710e$ ) and LP (1) N3  $\rightarrow$   $\pi^*$  C6-C10 ( $ED_j=0.38019e$ ) for C-1 were calculated as 55.68 and 39.15 kcal/mol, respectively, whereas the same interactions for C-2 were predicted by the energy of 51.72 and 39.44 kcal/mol. From Table 7, the interaction LP (3) Cl-1  $\rightarrow$   $\pi^*$  C12-C13 for C-1 was estimated with the  $E^{(2)}$  of 62.82 kcal/mol, whereas the energy of this interaction for C-2 was calculated smaller at 12.77 kcal/mol. In terms of the contribution of the chlorine substitution to lowering stabilization energy, the energies of the interactions LP (3) Cl-25 ( $ED_i=1.92058e$ )  $\rightarrow$   $\pi^*$  C12-C13 ( $ED_j=0.40956e$ ) and LP (2) Cl-28 ( $ED_i=1.96911e$ )  $\rightarrow$   $\pi^*$  C11-C14 ( $ED_j=0.37195e$ ) for C-1 were found to be 17.16 and 21.87 kcal/mol, respectively. On

TABLE 5: Drug-likeness scores and medicinal chemistry properties of oxindoles (C-1 and C-2).

Ligands	Drug-likeness rules						Medicinal chemistry		
	Lipinski	Ghose	Veber	Egan	Muegge	PAINS	Brenk	Lead likeness	Synthetic accessibility
C-1	Yes	Yes	Yes	Yes	Yes	0 alert	<b>2 alerts: michael_acceptor-, stilbene</b>	No; 1 violation: XLOGP3 > 3.5	2.52
C-2	Yes	Yes	Yes	Yes	Yes	0 alert	<b>2 alerts: michael_acceptor_1, stilbene</b>	No; 1 violation: XLOGP3 > 3.5	2.55

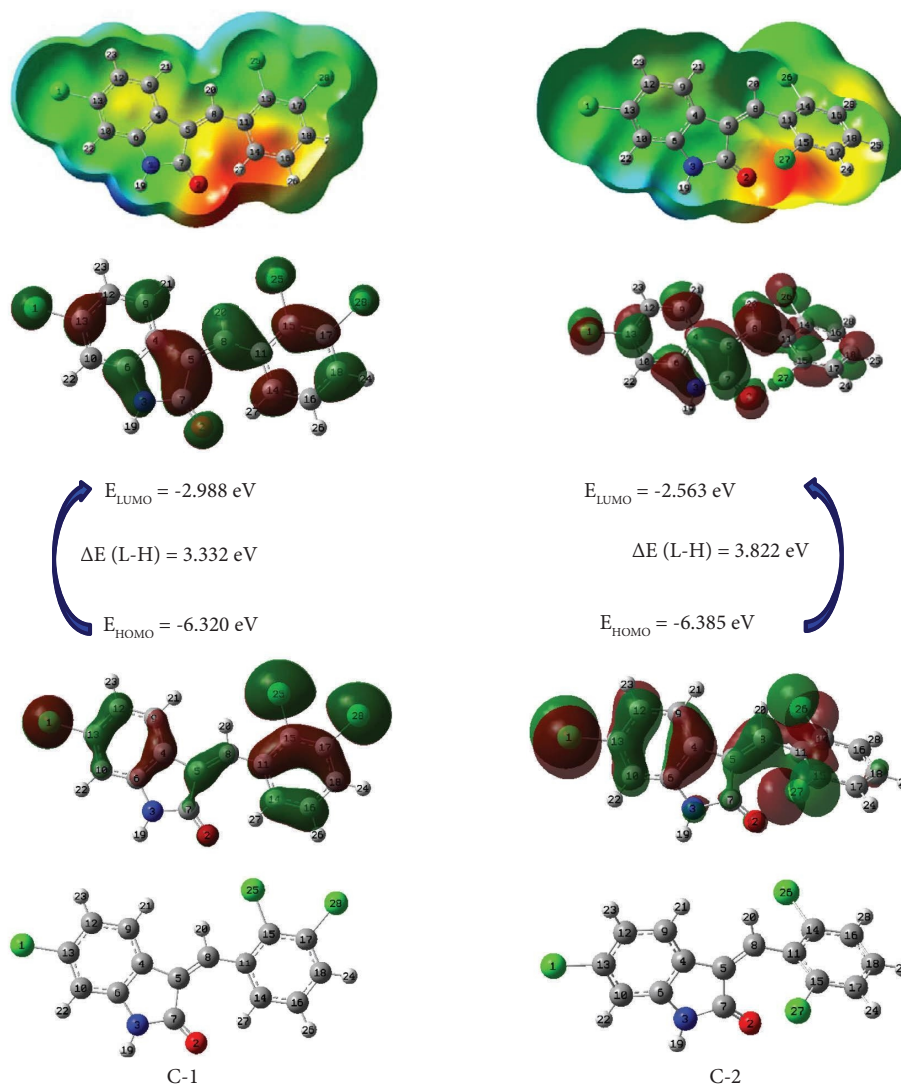


FIGURE 4: The optimized geometries, HOMO and LUMO plots (isoval: 0.02), and MEP graphs (isoval: 0.0004) of oxindoles (C-1 and C-2).

TABLE 6: The thermochemical and quantum chemical values of the compounds at the B3LYP/6-311++G\*\* level.

	C-1	C-2
<i>Physicochemical values</i>		
$\Delta E$ (au)	-2087.061203	-2087.060467
$\Delta H$ (au)	-2087.043669	-2087.042719
$\Delta G$ (au)	-2087.108101	-2087.107219
$\Delta E_{\text{thermal}}$ (kcal/mol)	130.145	129.694
$C_v$ (cal/molK)	63.475	63.975
$S$ (cal/molK)	135.608	135.751
DM (debye)	1.099939	1.035139
$\alpha$ (au)	261.327036	239.225564
<i>Quantum chemical values</i>		
H (-I) (eV)	-6.320	-6.385
L (-A) (eV)	-2.988	-2.563
$\Delta E$ (L-H) (eV)	3.332	3.822
$\mu$ (eV)	-4.654	-4.474
$\eta$ (eV)	1.666	1.911
$\omega$ (eV)	0.239	0.192
$\omega^+$ (au)	0.161	0.119
$\omega^-$ (au)	0.332	0.283
$\Delta N_{\text{max}}$ (eV)	2.793	2.341
$\Delta \epsilon_{\text{back-donat.}}$ (eV)	-0.417	-0.478

TABLE 7: NBO analysis results of compounds C-1 and C-2 at B3LYP/6-311++G\*\* level.

Donor (i)	ED <sub>i</sub> /e	Acceptor (j)	ED <sub>j</sub> /e	E <sup>(2)</sup> /kcalmol <sup>-1</sup>	E(j)-E(i)/a.u	F(i,j)/a.u
C-1						
$\pi$ C4-C9	1.65678	$\pi^*$ C6-C10	0.38019	22.72	0.28	0.072
		$\pi^*$ O2-C7	0.30710	17.92	0.28	0.065
$\pi$ C5-C8	1.79269	$\pi^*$ C4-C9	0.37830	14.07	0.31	0.062
		$\pi^*$ C11-C14	0.37195	12.26	0.27	0.054
$\pi$ C6-C10	1.66782	$\pi^*$ C4-C9	0.37830	16.07	0.30	0.063
$\pi$ C12-C13	1.68580	$\pi^*$ C4-C9	0.37830	19.31	0.30	0.069
		$\pi^*$ C6-C10	0.38019	16.27	0.29	0.062
$\pi$ C15-C17	1.71116	$\pi^*$ C11-C14	0.37195	16.03	0.29	0.062
$\pi$ C16-C18	1.64295	$\pi^*$ C11-C14	0.37195	22.97	0.25	0.068
LP (3) Cl-1	1.92472	$\pi^*$ C12-C13	0.40956	62.82	0.06	0.061
LP (1) N3	1.66411	$\pi^*$ O2-C7	0.30710	55.68	0.28	0.111
		$\pi^*$ C6-C10	0.38019	39.15	0.29	0.096
LP (3) Cl-25	1.92058	$\pi^*$ C12-C13	0.40956	17.16	0.69	0.109
LP (2) Cl-28	1.96911	$\pi^*$ C11-C14	0.37195	21.87	0.14	0.055
LP (3) Cl-28	1.92400	$\pi^*$ C11-C14	0.37195	7.22	0.17	0.034
C-2						
$\pi$ C4-C9	1.66347	$\pi^*$ C5-C8	0.11416	12.91	0.30	0.059
		$\pi^*$ C6-C10	0.37655	22.61	0.28	0.072
		$\pi^*$ C12-C13	0.40596	18.81	0.27	0.065
$\pi$ C5-C8	1.84371	$\pi^*$ O2-C7	0.27604	15.94	0.30	0.064
		$\pi^*$ C4-C9	0.37077	12.70	0.31	0.060
$\pi$ C6-C10	1.66571	$\pi^*$ C4-C9	0.37077	15.95	0.30	0.062
		$\pi^*$ C12-C13	0.40596	22.44	0.28	0.072
$\pi$ C12-C13	1.68851	$\pi^*$ C4-C9	0.37077	19.44	0.30	0.069
		$\pi^*$ C6-C10	0.37655	15.96	0.29	0.062
$\pi$ C15-C17	1.67164	$\pi^*$ C11-C14	0.41929	20.35	0.28	0.069
$\pi$ C16-C18	1.65770	$\pi^*$ C11-C14	0.41929	22.25	0.28	0.072
		$\pi^*$ C15-C17	0.37561	18.31	0.29	0.065
LP (3) Cl-1	1.92456	$\pi^*$ C12-C13	0.40596	12.77	0.33	0.063
LP (1) N3	1.66963	$\pi^*$ O2-C7	0.27604	51.72	0.29	0.110
		$\pi^*$ C6-C10	0.37655	39.44	0.29	0.096
LP (3) Cl-26	1.92536	$\pi^*$ C11-C14	0.41929	11.17	0.34	0.061
LP (3) Cl-27	1.92297	$\pi^*$ C15-C17	0.37561	5.16	0.60	0.054

the other hand, the corresponding interactions for C-2 were calculated as LP (3) Cl-26  $\rightarrow$   $\pi^*$  C11-C14 ( $E^{(2)} = 11.17$  kcal/mol) and LP (2) Cl-28  $\rightarrow$   $\pi^*$  C11-C14 ( $E^{(2)} = 5.16$  kcal/mol). On the other hand, the electron movement to the unfilled orbital of the fragment -C=O from the bond orbital C5-C8 had also a remarkable role in reducing stabilization energy. Accordingly, the energies of the interaction  $\pi$  C5-C8  $\rightarrow$   $\pi^*$  O2-C7 for C-1 and C-2 were calculated as 17.92 and 15.94 kcal/mol, respectively.

**3.8. Analysis of Electron Excitation Using Electron and Hole Density Distribution.** By comparing the ground state MO with the photoexcited states, we can see the differences in the electron density distribution maps (Figure 5). These maps displayed the spatial distribution of the electrons and gaps in the molecule, expressing details about the energy level of the excited state, the location and type of excited electrons, and the extent of electron delocalization.

**3.9. Topology Analysis.** To investigate the intramolecular interactions within these targeted derivatives, topological analysis of the atoms in each compound was implemented (Figure 6). Bond critical path (BCP), which manifests as blue

isosurface in the atoms in molecule (AIM) assessment, assures the occurrence of bonds between the atoms. Executed BCP for 2,3 and 2,6-dichloro indolinone is illustrated in Figure 6. In Figure 6, the blue dot in molecules revealed the presence of H-interaction at C-Cl...C=C. The total electron density  $\rho(r)$  and Laplacian  $\nabla^2\rho(r)$  values characterize bond constitution. Figure 6 proposes the occurrence of weak hydrogen bonding as blue dot between the O of the indolinone ring and phenyl rings. The isosurfaces appear between C=C...C<sub>6</sub>H<sub>4</sub> for both compounds, which is indicative of noncovalent hydrogen bond dynamic.

**3.10. Free Radical Scavenging Action in DPPH.** We observed the free radical scavenging activity of the prepared compounds (C-1 and C-2) in terms of DPPH. Table 8 displays the significant IC<sub>50</sub> values for both substances. In the DPPH activity, ascorbic acid was used as a reference medication with an IC<sub>50</sub> value of 293.10 M. Both the compounds caused significant scavenging effect against DPPH at various test concentrations ranging from 62.5 to 1000  $\mu$ M. The maximum inhibition for compound 1 was 91% at 1000  $\mu$ M with IC<sub>50</sub> of 37.390  $\mu$ M. Compound 2 illustrated maximum inhibition of 86% at 1000  $\mu$ M and IC<sub>50</sub> of 34.676  $\mu$ M.

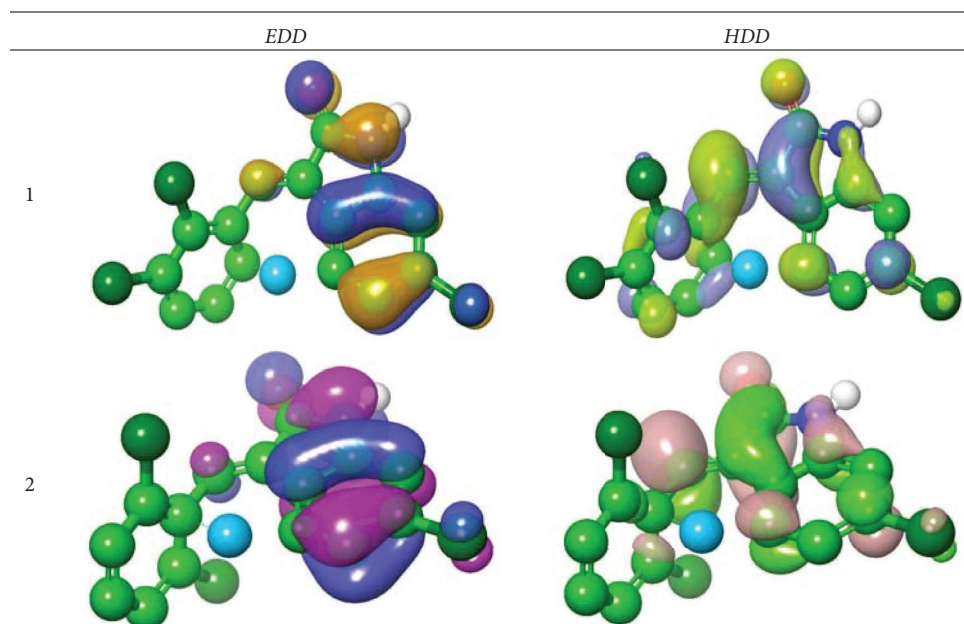


FIGURE 5: EDD and HDD profile for the excited state for compounds 2,3 and 2,6-dichloro indolinone derivatives.

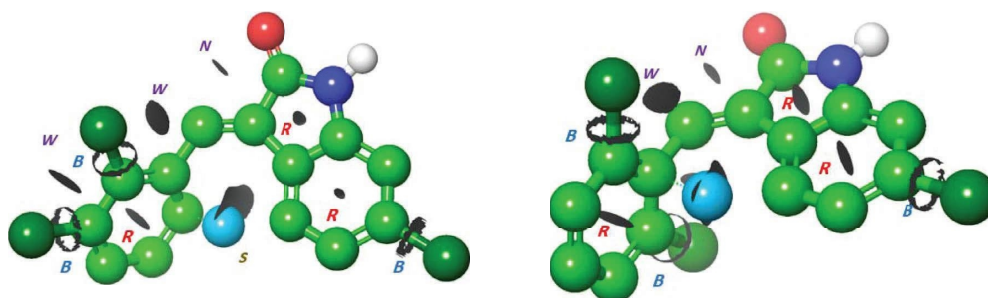


FIGURE 6: Interaction region indicator surfaces of C-1 and C-2 based on QTAIM analysis. B: BCP, R: RCP. Blue dot represents (S) strong interaction, and noncovalent interaction (N) and isosurface represent (w) weak interaction.

TABLE 8: Results of compounds (C-1 and C-2) for DPPH scavenging activity.

Compounds	Concentrations ( $\mu\text{M}$ )	Findings	% Inhibition	IC <sub>50</sub> ( $\mu\text{M}$ )
Control		$0.706 \pm 0.02845$		
Compound 1	1000	$0.066 \pm 0.00115^{**}$	91	37.390
	500	$0.09833 \pm 0.00203^{**}$	86	
	250	$0.151 \pm 0.00524^{**}$	79	
	125	$0.24067 \pm 0.01784^*$	66	
	62.5	$0.28533 \pm 0.01419^*$	60	
Compound 2	1000	$0.10 \pm 0.00651^{**}$	86	34.676
	500	$0.13466 \pm 0.02577^{**}$	81	
	250	$0.191 \pm 0.00681^{**}$	73	
	125	$0.25067 \pm 0.01995^*$	64	
	62.5	$0.29 \pm 0.05105^*$	59	
Standard	1000	$0.05367 \pm 0.00145^{**}$	92	29.363
	500	$0.07467 \pm 0.01586^{**}$	89	
	250	$0.143 \pm 0.01539^{**}$	80	
	125	$0.207 \pm 0.00436^{**}$	71	
	62.5	$0.263 \pm 0.00961^*$	63	

Inhibition percentages (%) and IC<sub>50</sub> values (mean  $\pm$  SEM of  $n=3$ ) are used to present the results. \* $P < 0.05$  significant; \*\* $P < 0.01$  significant.

**3.11. Free Radical Scavenging Activity in ABTS.** The results of the tested compounds, C-1 and C-2, in ABTS assay at various concentrations are displayed in Table 9. Overall, both the compounds exhibited significant scavenging activity. Compound 1 produced concentration-dependent inhibition with maximum effects of 88% at 1000  $\mu\text{M}$ , and the  $\text{IC}_{50}$  value was calculated as 25.381  $\mu\text{M}$ . Similarly, compound 2 showed 85% of maximum inhibition at highest test concentration at 1000  $\mu\text{M}$  with  $\text{IC}_{50}$  value calculated as 33.706  $\mu\text{M}$ . The standard (gallic acid) had  $\text{IC}_{50}$  value of 307.30  $\mu\text{M}$  in the ABTS test.

#### 4. Discussion

The primary goal of every research project is to discover novel and more potent compounds without compromising the safety issue. The present study evaluated the pharmacokinetic studies via SwissADME and stability through DFT studies of the newly synthesized compounds followed by antioxidant potential through in vitro assays.

Oxindoles are endogenous aromatic chemical molecules that are present in various natural products from plants as well as in the body fluids and tissue of mammals. They have a bicyclic structure and are aromatic heterocyclic organic molecules [3]. The name "oxindole" and its derivatives are defined as "1,3-dihydro-2H-indole-2-one(s)" because of the structure of the compound, which consists of a six-membered benzene ring combined with a five-membered pyrrole ring while C-2 position have a carbonyl group. Even though it is a familiar term, oxindole, is frequently used instead of its more scientific nomenclature, 2-indolinone [15, 27].

According to the traditional literature, oxindole has been used to treat inflammatory conditions such as arthritis, gastric ulcers, cancer, and infections [4]. Industry and academics have been attracted by its varied pharmacological profile to create novel synthetic oxindole derivatives with a range of biological functions. Sunitinib, a commercialized anticancer drug used to treat renal and gastrointestinal cancers, was made possible by the synthesis of synthetic oxindole derivatives [5]. Due to potential effects of indolidan and adibendan on cardiovascular system, they have also been used to treat congestive heart failure [28]. Spiro-oxindole derived compounds have been linked to a widespread biological actions, such as anticancer and antioxidant [29], anti-Alzheimer [30], kinase inhibitory activity [31],  $\beta_3$  adrenergic receptor agonist [32], antibacterial [33], neuroprotective [34], spermicidal [35], and analgesic activity [36].

The study aimed to synthesize two derivatives of 6-chlorooxindole, referred to as C-1 and C-2, by refluxing 6-chlorooxindole with 2,3-dichlorobenzaldehydes and 2,6-dichlorobenzaldehydes in ethanol with the addition of a catalytic amount of piperidine. The structures of C-1 and C-2 were characterized and confirmed by using  $^1\text{H}$  NMR,  $^{13}\text{C}$  NMR, and HR ESI mass spectroscopy.

Lipinski's rule of five is required for practical drug creation, according to the results of the pharmacokinetic investigation of the oxindole derivative compounds C-1 and C-2. Any medication molecule that breaks even one of the

requirements could have poor absorption or low permeability [37, 38]. The fraction of  $sp^3$  hybridized Cs in entire number of carbon atoms is defined as F.Csp3. It displays the complexity of the molecular spatial structure and represents the carbon saturation. F.Csp3 should be  $\geq 0.42$  because 84% of commercially available medicines meet this requirement [39]. The  $sp^3$  content must be increased, but only to a certain extent, as a higher F.Csp3 score is not a confirmation of high quality and may make chemical production more complex [40]. Natural goods are therefore a potential source of therapeutics because synthetic products often have a smaller percentage of F.Csp3 than do natural compounds [41]. As known well, the number of rotatable bonds greater than 10 tends to be more flexible and have higher entropy, making them more difficult to be absorbed by the body [42]. Although the count of the "rotatable bond filter" has not directly related to the rate of clearance in vivo, its mechanism of action is still unknown. This filter is justified, however, by the potential of in vitro screening due to the potency of ligand affinity drops at a rate of, on average, 0.5 kcal for every two rotatable bonds [43]. Both the H-bond-acceptor and the donor is still within range and thus H-bond acceptors, donors, and rotatable bonds are less frequent in oral medicines [44]. These three factors promote the oral mode of delivery as being adaptable, practical, and easy one.

As known well, a specific molecular system with a TPSA more than 140  $\text{\AA}^2$  would result in low absorption with fractional absorption less than 10%, whereas a TPSA of 60  $\text{\AA}^2$  would lead to strong absorption with fractional absorption greater than 90% [45]. Accordingly, the oxindoles (C-1 and C-2) could be potent agents to have better absorption as reflected by TPSA of 29.10  $\text{\AA}^2$ .

The consensus Log  $P_{o/w}$  known as the octanol/water partition coefficient is the average of the Log  $P_{o/w}$  calculated via the approaches of iLOGP, XLOGP3, WLOGP, MLOGP, and SILICOS-IT. Based on polarity, molecule size, and hydrogen bonding, a higher Log  $P_{o/w}$  number suggests greater lipophilicity. In this work, Log  $P_{o/w}$  values of C-1 and C-2 are predicted as 4.33, which reflects optimal lipophilicity. The Log  $P_{o/w}$  values demonstrate optimal lipophilicity (optimal:  $0 < \text{Log } P < 3$ ) [46]. Log S is the aqueous solubility of both compounds C-1 and C-2 which showed poor solubility in water. The SwissADME database showed that both compounds C-1 and C-2 had high GI absorption [45].

The C-1 and C-2 oxindole derivatives are expected to pass the blood-brain barrier. The chemicals (C-1 and C-2) that are oxindole derivatives are not p-glycoprotein substrates. This might not link them to interactions with various endogenous or exogenous substances, particularly medications. It is anticipated that the oxindole derivatives chemicals (C-1 and C-2) will not interact with P-glycoprotein, which may not have an impact on the pharmacological profile of other medications [47]. The majority of medications are metabolized by CYP3A4 which is one of the most critical isoforms of the CYP P450 and endogenous substances are projected to not affect CYP3A4, indicating a reduced frequency of interactions. Oxindole derivatives (C-1 and C-2) are projected to behave similarly, with no impact on

TABLE 9: Results of compounds (C-1 and C-2) for ABTS scavenging activity.

Compounds	Concentrations ( $\mu\text{M}$ )	Findings	% Inhibition	IC <sub>50</sub> ( $\mu\text{M}$ )
Control		0.65333 $\pm$ 0.01453		
Compound 1	1000	0.08167 $\pm$ 0.00203	88**	25.381
	500	0.102 $\pm$ 0.00751	84**	
	250	0.17133 $\pm$ 0.0109	74**	
	125	0.20833 $\pm$ 0.00924	68**	
	62.5	0.24133 $\pm$ 0.00328	63*	
Compound 2	1000	0.09533 $\pm$ 0.00176	85**	33.706
	500	0.14 $\pm$ 0.02183	79**	
	250	0.198 $\pm$ 0.0168	70**	
	125	0.23267 $\pm$ 0.00639	64*	
	62.5	0.267 $\pm$ 0.01332	59*	
Standard	1000	0.048 $\pm$ 0.00208	93**	26.522
	500	0.0692 $\pm$ 0.0283	90**	
	250	0.129 $\pm$ 0.00231	82**	
	125	0.14313 $\pm$ 0.09187	78**	
	62.5	0.23467 $\pm$ 0.00666	64*	

Inhibition percentages (%) and IC<sub>50</sub> values (mean  $\pm$  SEM of  $n=3$ ) are used to present the results. \* $P < 0.05$ ; \*\* $P < 0.01$ .

CYP2D6. The compounds C-1 and C-2 would be involved in drug design because of their pharmacokinetic characteristics in terms of their potencies for CYP1A2, CYP2C19, and CYP2C9 inhibitions. Here, the bioavailability scores implied a sufficient plasma concentration. The bioavailability and permeability are the keys in new drug discovery. As a result, a medication candidate is awarded a probability-based score if  $F > 10\%$  in vivo [48]. The drug similarity parameters are anticipated to be followed by the oxindole derivatives compounds (C-1 and C-2). Also, in the boiled-egg charts, the white area reflects intestinal absorption in humans, whereas the yellowish area shows CNS penetration. If a medicine is absorbed via a method other than the oral route, it would be seen in the gray region of the chart [14].

The oxindoles (C-1 and C-2) could present good GI absorption and would be suitable for intestinal absorption. The oxindole derivatives (C-1 and C-2) are expected to pass the blood-brain barrier, which indicates that they are not completely free of CNS toxicity. The fact that neither of the oxindole derivatives (C-1 and C-2) is a P-glycoprotein substrate implies favorably that they might not affect the pharmacological profile of other medicines. The oxindole derivatives (C-1 and C-2) are not included in the list of “ $\alpha$ -screen artifacts,” “frequent hitters,” and “reactive compounds” since they have “zero” PAINS (Pan Assay interference compounds) warning. During HTS, PAINS have an uncontrollable tendency to produce false positive findings. Although the process is unclear, they are connected to protein reactivity and noncovalent interactions [49]. As known well, SwissADME tools generate structural limits for the possible usage, or structural violation, in smart drug design in terms of pharmacokinetics via using the 105 fragments presented by Brenk et al. Thus, it could have revealed an issue-causing fragment present in a particular molecule [50]. Two groups have been detected by this structural alert such as stillbene group and Michael acceptor group in oxindole derivatives, which might be reactive and reduce the potential side effects [51]. Yet, this can be linked

to already accessible preclinical investigations that have been done. The ability of a molecule to act as a “lead” in the drug development process is represented by the lead likeness parameter. Due to their molecular weights being  $< 350$ , C-1 and C-2 are capable of lead likeness. These pharmacophores can be further changed to produce superior pharmacological outcomes on the basis of SAR. The chemicals (C-1 and C-2) that are oxindole derivatives have been produced in a laboratory. The SwissADME database’s assessment of its synthetic accessibility, however, is consistent with the reality. The oxindole derivatives compounds (C-1 and C-2) were given scores of 2.52 and 2.55 by the SwissADME database, indicating simple step processes for synthesis. The challenging synthetic methods are for compounds with scores of 10 [44].

The distribution of electrons and holes forms the foundation of the idea of multimolecular orbital excitation density in the receptors and their corresponding receptor anions. This concept reveals the characteristics of the excited state for the 2,3- and 2,6-dichloro indolinone derivatives. The electron and hole density distribution can also help us understand the electronic structure and properties of these molecules, as well as to the way that molecules recognize and bind in receptor-ligand. The excited state can be modeled by the excitation of an electron from an occupied to a virtual molecular orbital (MO). For both compounds 2,3- and 2,6-dichloro indolinone that were the subject of the investigation, the EDD map in Figure 5 shows a thicker surface at 6-chloroindolinone, indicating a higher electron density in the entire chloroindolinone ring for C-1 and C-2. HDD map for C-1 and C-2 shows a denser isosurface capped over ethylidenepyrrrolidinone core, which denotes a larger hole density.

The covalent, noncovalent, and electrostatic interactions are among the various forms of interactions that have an impact on compounds C-1 and C-2. Analysis using reduced density gradient (RDG) can identify and display non-covalent interactions (NCIs), employing a fluctuation of

gradient isosurfaces proportionate to the interaction intensity. The sign ( $\lambda_2$ )  $\rho$  values designates the bonding variety, where great negative quantities signify hydrogen bonding (blue dot), great positive quantities signify repulsive interactions (blue isosurface), and quantities near zero signify weak Van der Waals interactions (green isosurface) [50]. Simultaneously, the green isosurface indicated the presence of repulsive interaction present between pyrrolidine and phenyl rings for C1 and C2. The green color depicted the presence of weak Van der Waals interactions between Cl atom and C=C for C-2 compound. From these results, it is concluded that the manifestation of noncovalent interactions in the investigated compounds enhanced their stability in the biological media. The BCP associated with C=C...Cl in (2) and C...Cl in (1) corroborates the incidence of intramolecular interaction, which stabilizes the molecular structure. The strong interaction which is represented as blue dots was formed between carbonyl of indoline and C3 for benzene ring in both compounds, and other noncovalent interaction formed in 2,3- and 2,6-dichloro indolinone. Ring critical path (RCP) formed in three rings which appeared in the center for the surface of these rings.

## 5. Conclusion

In the current study, 6-chlorooxindole compounds C-1 and C-2 were prepared by refluxing 6-chlorooxindole with 2,3-dichlorobenzaldehydes and 2,6-dichlorobenzaldehydes in ethanol in the presence of a catalytic amount of piperidine, respectively. C-1 and C-2 showed greater GI absorption with good lipid solubility and pharmacokinetic properties.  $\Delta E$  (L-H) values revealed that C-1 could likely prefer the intramolecular interactions rather than the intermolecular interactions, and vice versa for C-2. Also,  $\Delta E_{\text{back-donat}}$  (eV) values indicated that C-2 (-0.478) would have gained stability more than C-1 (-0.417) via back donation. The NBO analysis disclosed that the  $n-\pi^*$  and  $\pi-\pi^*$  interactions would contribute to the stabilization of both compounds. In DPPH and ABTS assay, the compounds C-1 and C-2 both functioned as effective antioxidants. To sum up, the results obtained from in silico experiments followed by in vitro assays suggested significant therapeutic potential of these compounds.

## Data Availability

The data used to support the findings of this study are available from the corresponding author upon request.

## Conflicts of Interest

The authors declare that they have no conflicts of interest.

## Acknowledgments

The authors are grateful to the Scientific and Technological Research Council of Turkey (TUBITAK). All quantum chemical calculations were performed at the High Performance and Grid Computing Center (TR-Grid e-Infrastructure) and support of the Researchers Supporting

Project number RSPD2023R653 and King Saud University, Riyadh, Saudi Arabia.

## Supplementary Materials

Figure S1: NMR data. Figure S2: mass spectra of compounds (C1-C2). (*Supplementary Materials*)

## References

- [1] W. C. Sumpter, "The chemistry of oxindole," *Chemical Reviews*, vol. 37, no. 3, pp. 443–479, 1945.
- [2] S. Shah, Z. Ahmad, M. Yaseen et al., "Phytochemicals, in vitro antioxidant, total phenolic contents and phytotoxic activity of *Cornus macrophylla* Wall bark collected from the North-West of Pakistan," *Pakistan journal of pharmaceutical sciences*, vol. 28, no. 1, pp. 23–28, 2015.
- [3] M. Kaur, "Oxindole: a nucleus enriched with multitargeting potential against complex disorders," *Key Heterocycle Cores for Designing Multitargeting Molecules*, pp. 211–246, Elsevier, Amsterdam, Netherlands, 2018.
- [4] R. Roskoski, "Sunitinib: a VEGF and PDGF receptor protein kinase and angiogenesis inhibitor," *Biochemical and Biophysical Research Communications*, vol. 356, no. 2, pp. 323–328, 2007.
- [5] R. F. Kauffman, D. W. Robertson, R. B. Franklin et al., "Indolidan: a potent, long-acting cardiotoxic and inhibitor of type IV cyclic amp phosphodiesterase," *Cardiovascular Drug Reviews*, vol. 8, no. 4, pp. 303–322, 1990.
- [6] A. Phaniendra, D. B. Jestadi, and L. Periyasamy, "Free radicals: properties, sources, targets, and their implication in various diseases," *Indian Journal of Clinical Biochemistry*, vol. 30, no. 1, pp. 11–26, 2015.
- [7] Y. Hirata, C. Yamada, Y. Ito et al., "Novel oxindole derivatives prevent oxidative stress-induced cell death in mouse hippocampal HT22 cells," *Neuropharmacology*, vol. 135, pp. 242–252, 2018.
- [8] A. Toumi, S. Boudriga, K. Hamden et al., "Synthesis, anti-diabetic activity and molecular docking study of rhodanine-substituted spirooxindole pyrrolidine derivatives as novel  $\alpha$ -amylase inhibitors," *Bioorganic Chemistry*, vol. 106, Article ID 104507, 2021.
- [9] G. Serdaroglu and N. Uludağ, "The electronic and spectroscopic investigation of ( $\pm$ )- Dasycarpidone," *Vibrational Spectroscopy*, vol. 111, Article ID 103156, 2020.
- [10] J. S. Al-Otaibi, Y. S. Mary, Y. S. Mary, and G. Serdaroglu, "Adsorption of adipic acid in Al/BN/P nanocages: DFT investigations," *Journal of Molecular Modeling*, vol. 27, no. 4, pp. 113–117, 2021.
- [11] M. Khan, M. Yousaf, A. Wadood et al., "Discovery of novel oxindole derivatives as potent  $\alpha$ -glucosidase inhibitors," *Bioorganic and Medicinal Chemistry*, vol. 22, no. 13, pp. 3441–3448, 2014.
- [12] M. Frisch, G. Trucks, H. Schlegel et al., *Gaussian09 Revision D. 01*, Gaussian Inc, Wallingford UK, 2010.
- [13] R. Dennington, T. A. Keith, and J. M. Millam, *GaussView 6.0.16*, Semichem Inc, Shawnee Mission, KS, USA, 2016.
- [14] A. D. Becke, "A new mixing of Hartree-Fock and local density-functional theories," *The Journal of Chemical Physics*, vol. 98, no. 2, pp. 1372–1377, 1993.
- [15] I. Ahmad, H. Khan, and G. Serdaroglu, "Physicochemical properties, drug likeness, ADMET, DFT studies, and in vitro antioxidant activity of oxindole derivatives," *Computational Biology and Chemistry*, vol. 104, Article ID 107861, 2023.

- [16] R. Krishnan, J. S. Binkley, R. Seeger, and J. A. Pople, "Self-consistent molecular orbital methods. XX. A basis set for correlated wave functions," *The Journal of Chemical Physics*, vol. 72, no. 1, pp. 650–654, 1980.
- [17] J. P. Foster and F. Weinhold, "Natural hybrid orbitals," *Journal of the American Chemical Society*, vol. 102, no. 24, pp. 7211–7218, 1980.
- [18] E. Glendening, A. Reed, J. Carpenter, and F. Weinhold, *NBO Version 3.1*, Gaussian Inc, Wallingford, UK, 1998.
- [19] T. Koopmans, "Über die Zuordnung von Wellenfunktionen und Eigenwerten zu den einzelnen Elektronen eines Atoms," *Physica*, vol. 1, no. 1-6, pp. 104–113, 1934.
- [20] R. G. Pearson, "Absolute electronegativity and hardness correlated with molecular orbital theory," *Proceedings of the National Academy of Sciences*, vol. 83, no. 22, pp. 8440–8441, 1986.
- [21] R. G. Parr, L. V. Szentpály, and S. Liu, "Electrophilicity index," *Journal of the American Chemical Society*, vol. 121, no. 9, pp. 1922–1924, 1999.
- [22] J. L. Gázquez, A. Cedillo, and A. Vela, "Electrodonating and electroaccepting powers," *The Journal of Physical Chemistry A*, vol. 111, no. 10, pp. 1966–1970, 2007.
- [23] B. Gómez, N. V. Likhanova, M. A. Domínguez-Aguilar, R. Martínez-Palou, A. Vela, and J. L. Gázquez, "Quantum chemical study of the inhibitive properties of 2-pyridyl-azoles," *The Journal of Physical Chemistry B*, vol. 110, no. 18, pp. 8928–8934, 2006.
- [24] A. Sadiq, F. Mahmood, F. Ullah et al., "Synthesis, anticholinesterase and antioxidant potentials of ketoesters derivatives of succinimides: a possible role in the management of Alzheimer's," *Chemistry Central Journal*, vol. 9, no. 1, pp. 31–39, 2015.
- [25] G. Serdaroglu, N. Uludağ, E. Ercag, P. Sugumar, and P. Rajkumar, "Carbazole derivatives: synthesis, spectroscopic characterization, antioxidant activity, molecular docking study, and the quantum chemical calculations," *Journal of Molecular Liquids*, vol. 330, Article ID 115651, 2021.
- [26] R. Sakthivel, P. Sankudevan, P. Vennila, G. Venkatesh, S. Kaya, and G. Serdaroglu, "Experimental and theoretical analysis of molecular structure, vibrational spectra and biological properties of the new Co (II), Ni (II) and Cu (II) Schiff base metal complexes," *Journal of Molecular Structure*, vol. 1233, Article ID 130097, 2021.
- [27] Y. M. Khetmalis, M. Shivani, S. Murugesan, and K. V. G. Chandra Sekhar, "Oxindole and its derivatives: a review on recent progress in biological activities," *Bio-medicine and Pharmacotherapy*, vol. 141, Article ID 111842, 2021.
- [28] S. R. Yong, A. T. Ung, S. G. Pyne, B. W. Skelton, and A. H. White, "Synthesis of novel 3'-spirocyclic-oxindole derivatives and assessment of their cytostatic activities," *Tetrahedron*, vol. 63, no. 25, pp. 5579–5586, 2007.
- [29] D. Yasuda, K. Takahashi, T. Ohe, S. Nakamura, and T. Mashino, "Antioxidant activities of 5-hydroxyoxindole and its 3-hydroxy-3-phenacyl derivatives: the suppression of lipid peroxidation and intracellular oxidative stress," *Bioorganic and Medicinal Chemistry*, vol. 21, no. 24, pp. 7709–7714, 2013.
- [30] H. Watanabe, M. Ono, H. Kimura et al., "Synthesis and biological evaluation of novel oxindole derivatives for imaging neurofibrillary tangles in Alzheimer's disease," *Bioorganic and Medicinal Chemistry Letters*, vol. 22, no. 17, pp. 5700–5703, 2012.
- [31] J. Y. Lai, P. J. Cox, R. Patel et al., "Potent small molecule inhibitors of spleen tyrosine kinase (Syk)," *Bioorganic and Medicinal Chemistry Letters*, vol. 13, no. 18, pp. 3111–3114, 2003.
- [32] F. C. Stevens, W. E. Bloomquist, A. G. Borel et al., "Potent oxindole based human  $\beta_3$  adrenergic receptor agonists," *Bioorganic and Medicinal Chemistry Letters*, vol. 17, no. 22, pp. 6270–6273, 2007.
- [33] H. Singh, J. Sindhu, J. M. Khurana, C. Sharma, and K. Aneja, "Ultrasound promoted one pot synthesis of novel fluorescent triazolyl spirocyclic oxindoles using DBU based task specific ionic liquids and their antimicrobial activity," *European Journal of Medicinal Chemistry*, vol. 77, pp. 145–154, 2014.
- [34] S. Ingrand, L. Barrier, C. Lafay-Chebassier, B. Fauconneau, G. Page, and J. Hugon, "The oxindole/imidazole derivative C16 reduces in vivo brain PKR activation," *FEBS Letters*, vol. 581, no. 23, pp. 4473–4478, 2007.
- [35] P. Paira, A. Hazra, S. Kumar et al., "Efficient synthesis of 3, 3-diheteroaromatic oxindole analogues and their in vitro evaluation for spermicidal potential," *Bioorganic and Medicinal Chemistry Letters*, vol. 19, no. 16, pp. 4786–4789, 2009.
- [36] S. Chowdhury, M. Chafeev, S. Liu et al., "Discovery of XEN907, a spirooxindole blocker of NaV1.7 for the treatment of pain," *Bioorganic and Medicinal Chemistry Letters*, vol. 21, no. 12, pp. 3676–3681, 2011.
- [37] M. Pathak, H. Ojha, A. K. Tiwari, D. Sharma, M. Saini, and R. Kakkar, "Design, synthesis and biological evaluation of antimalarial activity of new derivatives of 2, 4, 6-s-triazine," *Chemistry Central Journal*, vol. 11, no. 1, pp. 132–211, 2017.
- [38] I. Ahmad, A. E. Kuznetsov, A. S. Pirzada, K. F. Alsharif, M. Daglia, and H. Khan, "Computational pharmacology and computational chemistry of 4-hydroxyisoleucine: physico-chemical, pharmacokinetic, and DFT-based approaches," *Frontiers in Chemistry*, vol. 11, pp. 1145974–1146015, 2023.
- [39] D. C. Kombo, K. Tallapragada, R. Jain et al., "3D molecular descriptors important for clinical success," *Journal of Chemical Information and Modeling*, vol. 53, no. 2, pp. 327–342, 2013.
- [40] E. M. Gerlach, M. A. Korkmaz, I. Pavlinov, Q. Gao, and L. N. Aldrich, "Systematic diversity-oriented synthesis of reduced flavones from  $\gamma$ -pyrones to probe biological performance diversity," *ACS Chemical Biology*, vol. 14, no. 7, pp. 1536–1545, 2019.
- [41] C.-Y. Jia, J.-Y. Li, G.-F. Hao, and G.-F. Yang, "A drug-likeness toolbox facilitates ADMET study in drug discovery," *Drug Discovery Today*, vol. 25, no. 1, pp. 248–258, 2020.
- [42] D. F. Veber, S. R. Johnson, H.-Y. Cheng, B. R. Smith, K. W. Ward, and K. D. Kopple, "Molecular properties that influence the oral bioavailability of drug candidates," *Journal of Medicinal Chemistry*, vol. 45, no. 12, pp. 2615–2623, 2002.
- [43] P. Andrews, D. Craik, and J. Martin, "Functional group contributions to drug-receptor interactions," *Journal of Medicinal Chemistry*, vol. 27, no. 12, pp. 1648–1657, 1984.
- [44] I. Ahmad, H. Khan, M. Usman Amin, S. Khalid, T. Behl, and N. Ur Rahman, "An overview on the anticancer potential of punarnavine: prediction of drug-like properties," *Oncologie*, vol. 23, no. 3, pp. 321–333, 2021.
- [45] A. Daina, O. Michielin, and V. Zoete, "SwissADME: a free web tool to evaluate pharmacokinetics, drug-likeness and medicinal chemistry friendliness of small molecules," *Scientific Reports*, vol. 7, no. 1, pp. 42717–42813, 2017.
- [46] M. Bitew, T. Desalegn, T. B. Demissie, A. Belayneh, M. Endale, and R. Eswaramoorthy, "Pharmacokinetics and drug-likeness of antidiabetic flavonoids: molecular docking and DFT study," *PLoS One*, vol. 16, no. 12, Article ID e0260853, 2021.

- [47] H. Zhang, H. Xu, C. R. Ashby, Y. G. Assaraf, Z. S. Chen, and H. M. Liu, "Chemical molecular-based approach to overcome multidrug resistance in cancer by targeting P-glycoprotein (P-gp)," *Medicinal Research Reviews*, vol. 41, no. 1, pp. 525–555, 2021.
- [48] Y. C. Martin, "A bioavailability score," *Journal of Medicinal Chemistry*, vol. 48, no. 9, pp. 3164–3170, 2005.
- [49] S. N. Bolz, M. F. Adasme, and M. Schroeder, "Toward an understanding of pan-assay interference compounds and promiscuity: a structural perspective on binding modes," *Journal of Chemical Information and Modeling*, vol. 61, no. 5, pp. 2248–2262, 2021.
- [50] A. Otero-De-La-Roza, E. R. Johnson, and J. Contreras-García, "Revealing non-covalent interactions in solids: NCI plots revisited," *Physical Chemistry Chemical Physics*, vol. 14, no. 35, pp. 12165–12172, 2012.
- [51] A. K. Singh, M. Bilal, D. Barceló, and H. M. Iqbal, "A predictive toolset for the identification of degradation pattern and toxic hazard estimation of multimeric hazardous compounds persists in water bodies," *Science of the Total Environment*, vol. 824, Article ID 153979, 2022.